ACS OMEGA

Open Access

This article is licensed under CC-BY-NC-ND 4.0

http://pubs.acs.org/journal/acsodf

Article

WS_2-Graphene van der Waals Heterostructure as Promising Anode Material for Lithium-Ion Batteries: A First-Principles Approach

T. K. Bijoy,* Sooryadas Sudhakaran, and Seung-Cheol Lee

Cite This: *ACS Omega* 2024, 9, 6482−6491

Read Online

ACCESS | Metrics & More | Article Recommendations | Supporting Information

ABSTRACT: In this work, we report the results of density functional theory (DFT) calculations on a van der Waals (VdW) heterostructure formed by vertically stacking single-layers of tungsten disulfide and graphene (WS2/graphene) for use as an anode material in lithium-ion batteries (LIBs). The electronic properties of the heterostructure reveal that the graphene layer improves the electronic conductivity of this hybrid system. Phonon calculations demonstrate that the WS2/graphene heterostructure is dynamically stable. Charge transfer from Li to the WS2/graphene heterostructure further enhances its metallic character. Moreover, the Li binding energy in this heterostructure is higher than that of the Li metal's cohesive energy, significantly reducing the possibility of Li-dendrite formation in this WS2/graphene electrode. *Ab initio* molecular dynamics (AIMD) simulations of the lithiated WS2/graphene heterostructure show the system's thermal stability. Additionally, we explore the effect of heteroatom doping (boron (B) and nitrogen (N)) on the graphene layer of the heterostructure and its impact on Li-adsorption ability. The results suggest that B-doping strengthens the Li-adsorption energy. Notably, the calculated open-circuit voltage (OCV) and Li-diffusion energy barrier further support the potential of this heterostructure as a promising anode material for LIBs.

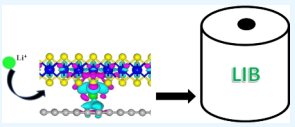

INTRODUCTION

Lithium-ion batteries (LIBs) are currently the most widely used energy source for portable electronics due to their superior capacity, high operational voltage, and long cycle life.[1] While well-established for mobile electronics, further performance improvements are necessary for their use in electric and hybrid electric vehicles.[2,3] The performance of an LIB primarily depends on its electrode materials. Transition metal oxides and phosphates are well-established cathode materials, while graphite and other carbon-based compounds are commonly used as anodes.[4−10] Graphite's excellent in-plane electrical conductivity, high structural stability, layered structure, and low cost make it a pivotal choice for LIB anodes. However, the main drawback is its low theoretical specific capacity (372 mAh/g).[11] Silicon (Si) is considered an alternative due to its high abundance and exceptional specific capacity. However, their poor electronic conductivity and massive volume expansion pose critical challenges. Reducing the dimensionality of bulk Si has shown some improvement, but commercialization remains difficult.[12] Therefore, finding alternative materials with high capacity, excellent electronic conductivity, and a durable cycle life is crucial. Graphene, the celebrated 2D material, exhibits high capacity in LIBs as it can store Li ions on both its sides and edges. Besides its rapid charge transport, graphene boasts an exceptional advantage for LIBs: the presence of the Dirac cone in its electronic structure. This unique feature allows electrons to behave as massless fermions, facilitating ultrafast movement.[13] Due to these intriguing physicochemical properties, graphene and graphene-containing compounds have found success as both anode and cathode materials in LIBs.[14,15] Beyond graphene, other 2D materials like silicene, hexagonal boron nitrides (*h*-BN), borophene, silicon carbides, transition metal dichalcogenides (TMDs), and MXenes have attracted attention for LIB applications.[16−23] Among these, TMDs have particularly enthralled battery researchers. Their diverse range can be synthesized from bulk phases through various methods like exfoliation, chemical vapor deposition, and supercritical assisted techniques.[24,25] TMDs follow the general formula MX2, where M represents a transition metal (e.g., V, Mo, W, Ta, Nb, or Re) and X symbolizes a chalcogenide (S, Se, or Te).[26−28] 2D-molybdenum disulfide (MoS2) stands as the flagship material among TMDs and has seen extensive research across various fields, including LIB applications.[29] Recently, 2D-WS2 has also garnered significant interest due to its striking structural similarities with MoS2. Notably, WS2 exhibits the same three crystal structures as MoS2:2H, 1T, and 3R.[30−32] For both TMDs, the 2H phase is the most stable and exhibits semiconducting properties. Single-layer 2H-TMDs are typically referred to as the 1H phase. Although the stable phase of TMDs possesses interesting physicochemical properties, its use in LIBs is hindered by low electronic conductivity. Additionally, some of these 2D materials bind weakly to Li ions. Addressing these drawbacks is crucial for their LIB applications.[33] Recent theoretical and experimental studies have shown that designing hybrid van der Waals (vdW)

Received: August 31, 2023
Revised: January 8, 2024
Accepted: January 12, 2024
Published: February 1, 2024

© 2024 The Authors. Published by American Chemical Society

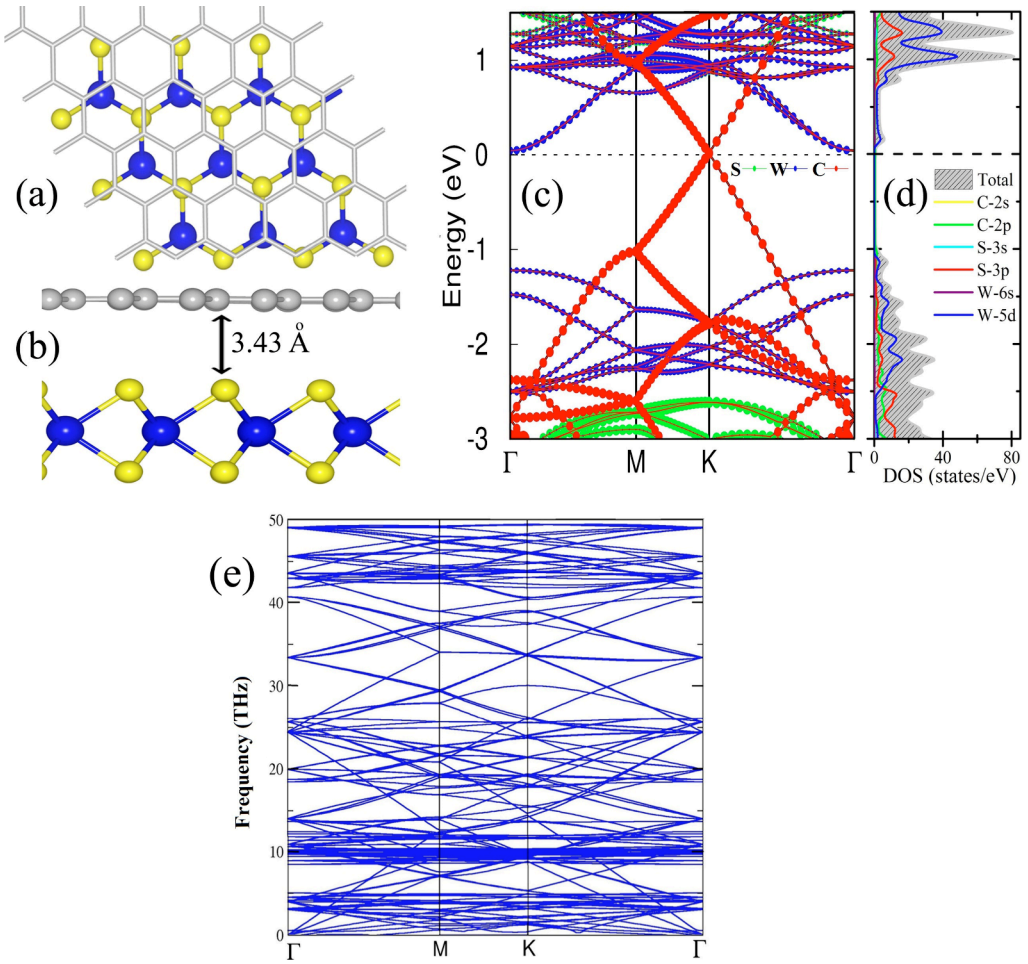

Figure 1. Ball and stick models of the optimized structure of (a) the 2H-WS_2-graphene heterostructure—top view, (b) the WS_2/graphene heterostructure—lateral view, (c, d) refers to the electronic partial band structure and density of states, and (e) the phonon band structure of the heterostructure, respectively. The yellow, blue, and gray balls denote sulfur, tungsten, and carbon atoms, respectively. The ball and stick models were generated using VESTA software.[53]

heterostructures by combining TMDs with graphene is an effective way to improve their electrochemical performance. For example, MoS2-graphene heterostructures demonstrate superior electrochemical performance to their individual components.[34−36] While research on MoS2-based heterostructures is extensive, studies on WS2-based structures are still in their infancy. However, the low cost, lower toxicity, and high abundance of WS2 make it a promising alternative to MoS2 among 2D chalcogenides.[37] Similar to the development of MoS2-based vdW heterostructures for diverse applications,[38] there are experimental reports exploring WS2-C composites as LIB anode materials.[39,40] However, an atomic-level understanding of these systems remains unclear. In this work, using first-principles DFT calculations, we investigate vertically stacked WS2/graphene heterostructures as potential LIB anodes. Our results show that this heterostructure is stable and exhibits enhanced Li-adsorption energy. Charge transfer from Li further improves the metallic character of the heterostructure. Moreover, the Li-diffusion barrier and OCV are suitable for LIB anode applications, even surpassing those of many established materials. We believe this study will inspire battery researchers to explore similar electrode materials in the near future.

COMPUTATIONAL METHODOLOGY

In this work, all the computations were performed using the first-principles-based DFT as implemented in the Vienna *Ab initio* Simulation Package (VASP).[41] Here, all the atoms are described by projector-augmented wave (PAW) pseudopotential, we have used generalized gradient approximations (GGA) to treat the exchange correlation.[42] All of the ions are relaxed without considering any symmetry, and the iterative relaxation processes are carried out until Hellmann−Feynman forces on each ion are converged to less than 0.01 eV/Å. For the optimization of the WS_2/graphene heterostructure, we have chosen G-point sampling with k-points of 5 × 5 × 1. To understand the effect of van der Waals interaction, we have used nonlocal DFT-D3 functional throughout calculations.[43] The convergence of energy is set to be 10^{-6} eV in all of the calculations. To avoid the interaction of this heterostructure with its periodic image along the *c*-axis, we kept sufficiently large vacuum (≈15 Å) along this direction. We have also performed the spin-polarized calculations in all the cases, to compare the magnetic and nonmagnetic solutions, but results show that system prefers to be stabilized in nonmagnetic solutions. Further, denser k-points (45 × 45 × 1) are used for deducing the electronic density of states (DOS) calculations. Further, we also calculated Bader charges for all the system to

https://doi.org/10.1021/acsomega.3c06559
ACS Omega 2024, 9, 6482−6491

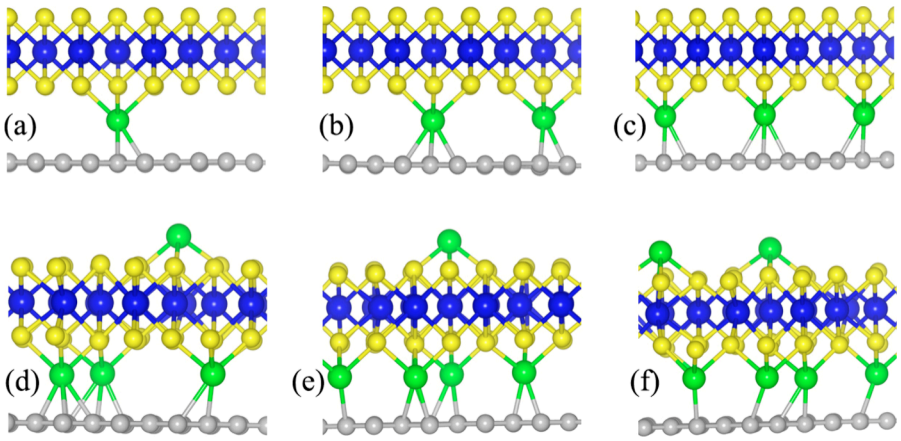

Figure 2. Ball and stick models of the optimized structure of (a) Li, (b) 2Li, (c) 3Li, (d) 4Li, (e) 5Li, and (f) 6Li added to the WS_2/graphene heterostructure. The yellow, blue, gray, and green colored balls represent sulfur, tungsten, carbon, and lithium atoms, respectively.

understand the charge transfer in this heterostructure.[44,45] Eventually, to investigate the energy barrier associated with the diffusion of Li ions through the heterostructure, we used the climbing image nudged elastic band (CI-NEB) method, as implemented in the VASP code.[46] Moreover, the *ab initio* molecular dynamics (AIMD) of the structure of the system has been calculated to understand the thermal stability of the heterostructure during lithiation. The dynamic stability of the heterostructure has been calculated using Phonopy code.[47]

RESULTS AND DISCUSSION

We began by optimizing the unit cell models of single-layer graphene and 1H-WS2 by using first-principles calculations. Our obtained lattice constants for graphene and WS2 ($a = b =$ 2.46 and 3.17 Å, respectively) agree well with previous reports.[48−51] However, these lattice parameters reveal a significant lattice mismatch of 22.4%, which would create challenges when stacking the materials. To address this mismatch, we constructed supercell models for both graphene and WS2. A (4 × 4) supercell for graphene and a (3 × 3) supercell for WS2 (see Figure S1 in the Supporting Information) were chosen, resulting in a manageable lattice mismatch of only ∼3.3%, which is generally acceptable for vdW heterostructures.[52] These optimized layers were then vertically stacked to form the WS2/graphene vdW heterostructure (Figure 1). The final structure remains periodic along the a- and b-directions, with sufficient vacuum space added along the c-direction to prevent interactions with neighboring unit cells. The optimized lattice parameter for the heterostructure is $a = b = 9.78$ Å (see Figure S2 in the Supporting Information). C−C and W−S bond lengths remained unchanged from those of the isolated layers, at 1.42 and 2.45 Å, respectively. Additionally, we optimized the equilibrium interlayer distance (ILD) between graphene and WS2 (Figure S3 in the Supporting Information) using DFT-D3 correction, ultimately obtaining a value of 3.43 Å, comparable to other established 2D materials. This interlayer distance plays a crucial role in the heterostructure's stability. Now, we turn our attention to the binding energy per atom (E_b), which is a key parameter for assessing the stability of any vdW heterostructure. The E_b is calculated as,

$$E_b = \frac{[E(\mathrm{WS_2/graphene}) - E(\mathrm{WS_2}) - E(\mathrm{graphene})]}{N} \quad (1)$$

Here, $E(\mathrm{WS_2/graphene})$, $E(\mathrm{WS_2})$, and $E(\mathrm{graphene})$ are the dispersion corrected total energies of the WS_2/graphene heterostructure, WS_2, and graphene, respectively. N denotes the total number of atoms present in the system (=59, in this case).

Our calculations reveal a fairly strong and energetically stable interaction between the WS2 and graphene layers, evident from the binding energy of −0.07 eV/atom. The charge density difference plot (Figure S4) further supports this, showcasing attractive binding interactions. To understand the impact of stacking on electronic properties, we analyzed the band structure and density of states (DOS) of the heterostructure (Figure 1c,d). Interestingly, the Dirac cone from pristine graphene remains intact at the Fermi level, ensuring a high electronic conductivity for this heterostructure. Moreover, the WS2 bands are significantly modified in the heterostructure. The conduction band minimum (CBM) and the valence band maximum (VBM) at the Brillouin zone center (Γ-point) shift closer, leading to a bandgap reduction from 1.81 eV in pristine WS2 to 1.10 eV in the heterostructure (Figure S4). This favorable narrowing likely arises from the van der Waals interaction between WS2 and graphene. Further analysis of the charge density (Figure S5) reveals charge polarization at the face-to-face sites, potentially facilitating efficient charge transfer from lithium to the heterostructure during lithiation, similar to observations in MoS2/graphene heterostructures.[38] Notably, this reduced bandgap is advantageous for LIB applications as it promotes faster lithium-ion mobility. Finally, phonon calculations (Figure 1e) confirm the structural and mechanical stability of the WS2/graphene heterostructure, evident by the absence of imaginary frequencies in the phonon band structure.

To gain insights into the lithiation process of the WS2/graphene heterostructure, we sequentially introduced Li atoms to various potential sites on the WS2 surface. We broadly considered three possibilities: (i) above the WS2 surface, (ii) at the interface between WS2 and graphene, and (iii) above the graphene layer (see Figure S6 in the Supporting Information). Our analysis revealed that added Li atoms can interact with WS2 in three distinct ways, regardless of their location (surface, interface, or above WS2): (a) binding to a "T_W-

https://doi.org/10.1021/acsomega.3c06559
ACS Omega 2024, 9, 6482−6491

Table 1. Lattice Parameters, Interlayer Distance (I_d), Average W−Li, S−Li, C−Li, and W−W Bond Distances, and Li-Adsorption Energies (E_{ad}) in the WS_2/Graphene Heterostructure

system	A (Å)	B (Å)	I_d (Å)	W−Li (Å)	S−Li (Å)	C−Li (Å)	C−C	W−S (Å)	W−W (Å)	E_{ad}
WS_2/graphene	9.78	9.78	3.43				1.43	2.43		
WS_2/graphene-Li	9.80	9.80	3.50	3.02	2.43	2.37	1.43	2.43		−2.43
WS_2/graphene-Li_2	9.81	9.81	3.53	3.04	2.44	2.36	1.43	2.43		−2.33
WS_2/graphene-Li_3	9.83	9.83	3.61	3.03	2.44	2.36	1.43	2.43		−2.11
WS_2/graphene-Li_4	9.83	9.83	3.50	2.99	2.42	2.37	1.43	2.43		−2.03
WS_2/graphene-Li_5	9.84	9.84	3.52	2.98	2.41	2.39	1.43	2.43		−2.01
WS_2/graphene-Li_6	9.85	9.85	3.49	2.95	2.39	2.42	1.43	2.43		−1.99

site"—a hollow site surrounded by three sulfur atoms and one tungsten atom; (b) binding to a "T_S-site"—a hollow site formed by three sulfur atoms; and (c) binding to a bridge "T_B-site" (see Figure S7 in the Supporting Information). Therefore, we investigated all of these possibilities for Li placement at the interface and above the WS2 layer. The most favored site for Li-adsorption is determined by calculating the Li-adsorption energy (E_{ad}) as,

$$E_{ad} = \frac{[E(WS_2/\text{graphene\_}n\text{Li}) - E(WS_2/\text{graphene}) - nE(\text{Li})]}{n} \quad (2)$$

where $E(WS_2/\text{graphene\_}n\text{Li})$ is the total energy of lithiated WS_2/graphene, $E(WS_2/\text{graphene})$ is the total energy of nonlithiated WS_2/graphene heterostructure, $E(\text{Li})$ is the atomic energy of Li atom, and n denotes to the total number of added Li to the heterostructure. The calculated adsorption energies for the addition of the first Li atom were −1.88 eV for case (i) (above the WS2 surface), −2.43 eV for case ii (at the interface), and −2.01 eV for case iii (above the graphene layer). These results clearly demonstrate that the interface of the heterostructure is energetically the most favorable site for Li adsorption.

Due to the presence of nine tungsten atoms in the system, there are nine possible "top of W" (TW) sites at the interface where Li could bind, facing different carbon atoms on the graphene (illustrated in Figure S8, Supporting Information). To identify the most stable configuration, we investigated nine different arrangements of Li at these TW sites. Figure 2 presents the most stable structure for Li intercalated into the WS2/graphene interface, and Table 1 summarizes its key structural details. Upon Li incorporation, the lattice parameters along the a and b directions increase slightly, as does the interlayer distance (IL) from 3.43 to 3.50 Å. Interestingly, the added Li interacts simultaneously with sulfur, tungsten, and carbon atoms in the heterostructure, with bond lengths of 2.43, 3.02, and 2.37 Å, respectively. Furthermore, we compared the Li-adsorption energy of the heterostructure with that of Li on bilayer WS2 and bilayer graphene (homostacked layers, depicted in Figure S9). On the individual layers, adsorption energy values were found to be −2.07 eV for bilayer WS2 and −1.76 eV for bilayer graphene. These results demonstrate that the WS2/graphene heterostructure exhibits superior Li-adsorption capability compared with its parent components, highlighting its potential as a promising anode material for LIBs. We further investigated the lithiation process by sequentially introducing more Li atoms (up to n = 6) into the heterostructure. The resulting stable structures are listed in Figure 2. Interestingly, the figure reveals that, for $n \leq 3$, all Li atoms occupy the interlayer region. However, for higher Li content (n >3), some Li atoms preferentially reside on top of the WS2 layer. Notably, in all investigated cases, no clustering of Li atoms was observed, indicating that they remained well separated from each other.

Calculated adsorption energies for n = 2 to 6 Li atoms range from −2.33 to −1.99 eV. Notably, this range consistently exceeds the cohesive energy of bulk lithium metal (1.70 eV). This implies that the intercalated Li atoms are strongly bound to the heterostructure and are less likely to cluster on the electrode surface. Preventing Li-ion clustering on the WS2/graphene electrode effectively suppresses the formation of Li dendrites, thereby enhancing the safety of LIBs. Furthermore, formation energy calculations for metal ion adsorption, as proposed by Liu et al., could provide valuable insights into the behavior of different metals absorbed onto this heterostructure.[54] This method is reportedly more quantitatively accurate than previous approaches. The formation energy for the Li-intercalated compound is calculated using the following equation,

$$\text{FE} = E_{ad} + E_d + E_s \quad (3)$$

Here, E_{ad}, E_d, and E_s are adsorption energy, lattice strain energy, and Li-atomization energy, respectively. Here, all of the calculated formation energies are negative, demonstrating the energetic feasibility of lithiation within the WS2/graphene heterostructure. Among the three factors involved in FE calculations, lattice deformation and Li-adsorption energy emerge as the most influential. Figure 3 illustrates the

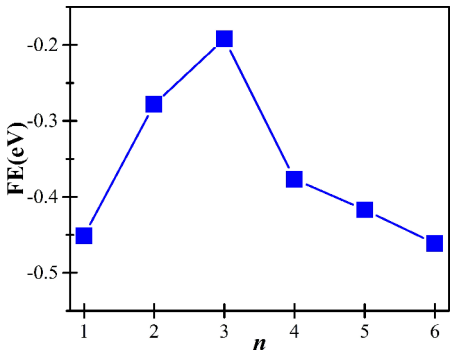

Figure 3. Number of Li vs formation energy plot for the lithiation of the WS_2/graphene heterostructure.

variations in the FE during lithiation. Notably, the FE initially increases from −0.3 eV for the first Li atom to −0.2 eV for the second. However, it subsequently declines for further lithiation (n = 3 and beyond). This trend deviates from the steadily decreasing Li-adsorption energy, underscoring the significant role of lattice deformation in shaping the overall FE of the lithiated system. Therefore, both Li-adsorption and lattice

https://doi.org/10.1021/acsomega.3c06559
ACS Omega 2024, 9, 6482−6491

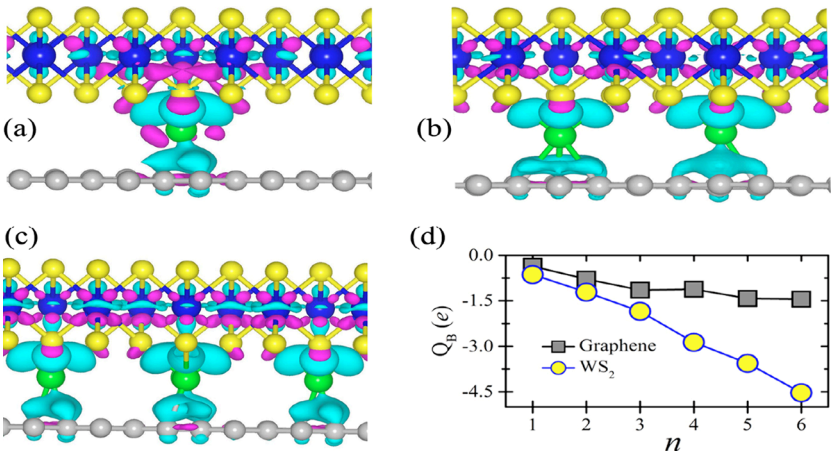

Figure 4. Charge density difference plot of the (a) 1Li, (b) 2Li, and (c) 3Li intercalated WS_2/graphene heterostructure, respectively. The cyan (magenta) isosurfaces correspond to an excess (depletion) of charge densities. The Bader charges of the lithiated WS_2/graphene heterostructure are given in panel d. In panel d, Q_B corresponds to charge transfer obtained using Bader charge analysis.

deformation effects must be carefully considered to accurately determine the FE of lithiated heterostructures.

Motivated by these findings, we investigated the effect of a higher Li concentration on the WS2/graphene heterostructure. To achieve this, we placed additional Li atoms on both the previously identified active sites and top graphene layer for an increased capacity. The relaxed structures with elevated Li content (n = 18−27) are presented in Figure S10 (refer to the Supporting Information). Notably, despite the significantly increased Li concentration, the adsorption energies remained consistently (−1.88 and −1.70 eV range), which are higher than the cohesive energy of the bulk lithium metal. Additionally, the lithiation process induced negligible changes in the heterostructure's lattice constants, with the maximum expansion observed for n = 27 being only 1.84%—well within the acceptable range for electrode materials. Interestingly, we observed the formation of localized W−W bonds (Figure S11, Supporting Information), likely arising from the reduction of WS2 to W due to charge transfer from Li. However, these W−W bonds remained isolated, allowing the added Li atoms to comfortably reside within the heterostructure without causing significant structural distortion. Further exploring the potential for enhanced Li adsorption, we investigated the effect of modifying the graphene layer through boron (B) and nitrogen (N) doping at the carbon sites. Our calculations revealed that B-doping significantly increased the Li-adsorption energy (−3.12 eV) compared to the reduced E_{ad} observed in N-doped WS2/graphene (−2.09 eV). These results suggest that B-doping presents a promising avenue for boosting Li adsorption, while N doping may not be advantageous in this context. To gain insight into the charge transfer process within the lithiated WS2/graphene heterostructure, we conducted both charge density difference mapping and Bader charge analysis. The results are presented in Figure 4. The charge density difference can be calculated as,

$$\Delta\rho = \rho(\mathrm{WS_2/graphene\_}n\mathrm{Li}) - \rho(\mathrm{WS_2/graphene}) - \rho(n\mathrm{Li}) \quad (4)$$

Here, $\rho(\mathrm{WS_2/graphene\_}n\mathrm{Li})$, $\rho(\mathrm{WS_2/graphene})$, and $\rho(n\mathrm{Li})$ represent the charge densities of lithiated heterostructure, pristine heterostructure, and added Li atoms, respectively.

Figure 4a−creveals a consistent pattern of charge transfer in all cases—from the intercalated Li atoms to the WS2/graphene heterostructure. This transfer strengthens the binding between the layers. Notably, the charge density plots show a greater accumulation of negative charge near the WS2 side compared to that near graphene, suggesting a preferential gain of electrons by WS2 from the Li atoms. To confirm this observation quantitatively, we performed Bader charge analysis, as shown in Figure 4d. Consistent with the visual findings, the analysis reveals that each intercalated Li atom completely donates its $2s^1$ valence electron to the heterostructure. The complete transfer of the 2s electrons from the Li atoms to the heterostructure indicates their strong polarization after adsorption. Notably, carbon, tungsten, and sulfur atoms in the heterostructure accept electrons from the Li atoms. To further analyze the charge distribution, we separated the Bader charge of the lithiated heterostructure into two components: "Q_B", denoting the total charge transfer, and the Bader charges of graphene and WS2 (calculated by summing the Bader charges of W and S). Figure 4d illustrates this breakdown. The figure clearly shows that the Bader charge of WS2 exceeds that of graphene in all cases. Among the individual atoms within WS2, those directly interacting with Li (sulfur atoms) receive the majority of the transferred charge, followed by carbon and tungsten. This preferential transfer to sulfur stems from its higher electronegativity compared with carbon and tungsten. To investigate the impact of lithiation on the electronic properties of the WS2/graphene heterostructure, we calculated the electronic density of states (DOS), presented in Figure 4. The density of states (DOS) in Figure 5 reveals the metallic nature of the lithiated WS2/graphene heterostructure due to states crossing the Fermi energy (E_f). This transition from a semimetallic to a metallic character is directly attributed to the electron transfer from Li to the heterostructure, as confirmed by the Bader charge analysis earlier. Notably, the total and partial DOS plots also show a gradual shift toward the lower energy region (stronger bonding) with increasing Li content. This trend is particularly evident for the W-5d, S-3p, and C-2p states, further supporting the Bader charge analysis findings. Overall, the DOS analysis suggests that introducing Li to the WS2/graphene heterostructure enhances its electronic conductivity. Additionally, the shift toward lower energies indicates increased electronic stability of the lithiated system.

https://doi.org/10.1021/acsomega.3c06559
ACS Omega 2024, 9, 6482−6491

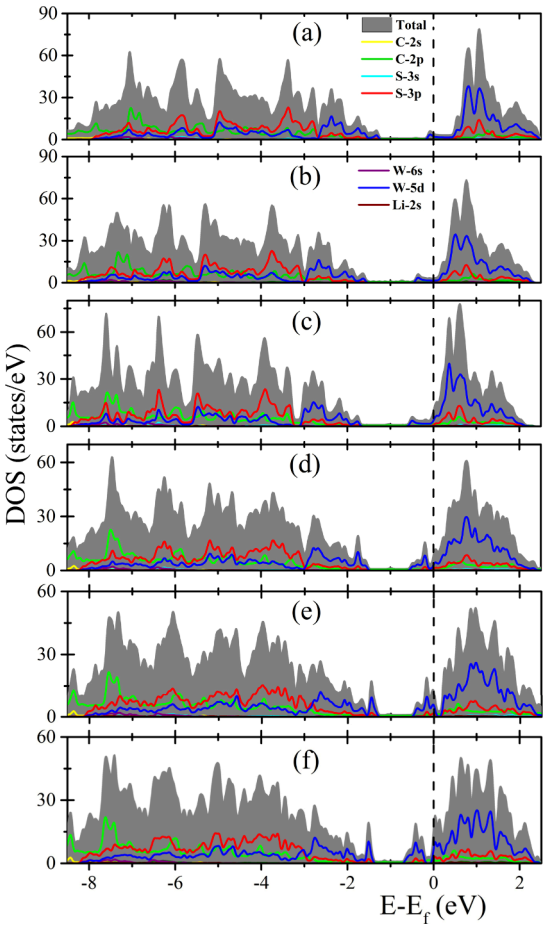

Figure 5. Total and angular momentum resolved electronic density of states of the (a) WS_2/graphene-Li, (b) WS_2/graphene-2Li, (c) WS_2/graphene-3Li, (d) WS_2/graphene-4Li, (e) WS_2/graphene-5Li, and (f) WS_2/graphene-6Li heterostructure, respectively. The dashed line refers to the Fermi energy.

Beyond the density of states, we further investigated the electronic properties through band structure calculations, shown in Figure 6. These results offer deeper insights into the impact of Li doping. Interestingly, introducing a single Li atom partially pushes the Dirac cone of graphene, altering the band structure. Additionally, the conduction band minimum (CBM) of WS2, located at the Γ-point, also exhibits a partial shift toward the bonding region upon lithiation. These observations again lend support to the previously discussed charge transfer from Li to both graphene and WS2. Furthermore, as the Li concentration increases, the upper half of the Dirac cone (previously unoccupied) becomes entirely filled. Notably, the number of bands crossing the Fermi energy increases with lithiation, further confirming the enhanced metallic character of the WS2/graphene electrode.

Further analysis of the band structures reveals interesting observation, which is a narrow band gap opens at the Dirac point where the heterostructure interacts with Li atoms. The gap size ranges from 7.2 to 32.6 meV, as shown in Figure S12 (Supporting Information). Intriguingly, beyond a Li concentration of n = 3, the Dirac cone's position and observed band gap remain relatively constant. This suggests that charge transfer from Li to graphene saturates beyond n = 3, as supported by the Bader charge analysis in Figure 4d. While graphene's charge gain shows slight variation (−0.36 to −1.45 e), WS2 experiences a much more significant increase (−0.64 to −4.54 e). This observation implies that Li atoms preferentially interact with the WS2 side (either top layer or interface) rather than the top graphene layer. Only when these preferable sites are filled (for Li >18) do Li atoms occupy the top graphene layer.

Another intriguing feature observed in the band structures of the lithiated WS2/graphene heterostructure is the emergence of a discrete band that appears beyond n = 3. To understand the origin of this localized band, we performed band-decomposed charge density calculations for the representative case of 4Li-added WS2/graphene. We focused on the energy range in which this band is distributed. The results reveal that this distinct band originates from three specific W atoms, as visualized in Figure 7. Interestingly, the average distance between these three W atoms is 3.56 Å, exceeding the typical W−W bond length of 3.26 Å.

To assess the thermal stability of the lithiated WS2/graphene heterostructure, we conducted *Ab Initio* Molecular Dynamics (AIMD) simulations under the NVT ensemble at 300 K. This approach has proven effective for understanding the thermodynamic stability of various van der Waals heterostructures.[55,56] The results are presented in Figure 8. The AIMD simulations reveal only negligible energy fluctuations throughout the simulation period, indicating a highly stable structure. While some minor dislocations are observed, no ruptures of W−S bonds occur at this temperature. This finding aligns with previous AIMD studies demonstrating the inherent stability of lithiated WS2/graphene heterostructures.[57]

To delve deeper into the electrochemical performance of the WS2/graphene electrode, we calculated its open-circuit voltage (OCV). The OCV can be calculated as,

$$\mathrm{OCV} = -[E(\mathrm{WS_2/graphene\_}n_2\mathrm{Li}) - E(\mathrm{WS_2/graphene\_}n_1\mathrm{Li}) - (n_2 - n_1)\mu(\mathrm{Li})]/(n_2 - n_1) \quad (5)$$

Here, (WS_2/graphene_n_2Li), E(WS_2/graphene_n_1Li), and μ(Li) represent the energies of n_2 and n_1 number Li added WS_2/graphene heterostructure, and chemical potential of bulk Li metal, respectively. Figure 9 presents the calculated OCV profile. The voltage varies from 0.55 to 0.25 V for n = 1 to 6 Li atoms. Interestingly, higher Li concentrations lead to a significant decrease in the lithiation−delithiation potential. Notably, the OCV approaches 0 V for n = 27. Considering all of the data points, the average voltage stabilizes at 0.18 V, which falls within the typical range for LIB anode materials. This confirms the suitability of the lithiated WS2/graphene heterostructure as an LIB anode. Furthermore, its average OCV surpasses that of many other reported 2D heterostructures, such as HfS2/graphene, h-BN/black phosphorene, and blue phosphorene/MS2 (M = Ta, Nb).[58−60] The lower OCV of this electrode opens up exciting possibilities for pairing it with high-voltage cathode materials like LiCoO2, paving the way for the design of high-voltage LIBs. Furthermore, we calculated the theoretical specific capacity of the WS2/graphene heterostructure for a 1:1 Li stoichiometry (further details in the Supporting Information). Our calculations revealed a maximum achievable capacity of 588.16 mAh/g.

While the OCV profile serves as a valuable indicator of an electrode material's nature, a LIB's performance, particularly its charge−discharge rate, critically depends on lithium-ion

https://doi.org/10.1021/acsomega.3c06559
ACS Omega 2024, 9, 6482−6491

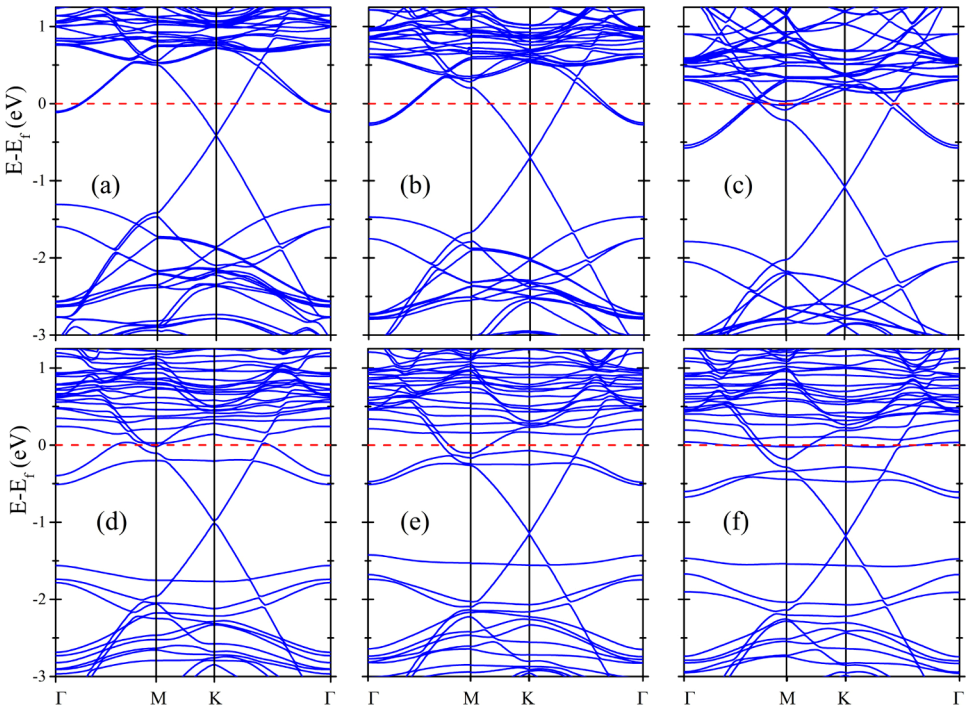

Figure 6. Electronic band structures of the (a) WS_2/graphene-Li, (b) WS_2/graphene-2Li, (c) WS_2/graphene-3Li, (d) WS_2/graphene-4Li, (e) WS_2/graphene-5Li, and (f) WS_2/graphener-6Li heterostructure, respectively. The dashed line refers to the Fermi energy.

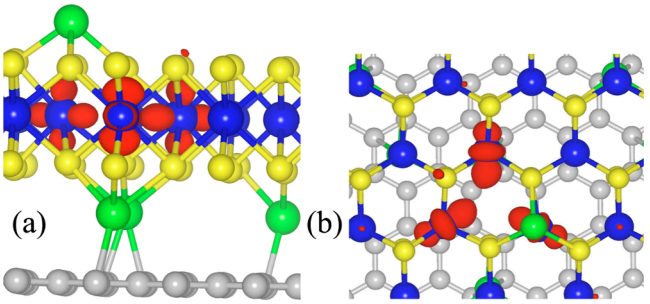

Figure 7. Lateral (a) and top (b) view of the band-decomposed charge density plot for the 4Li-added WS_2/graphene heterostructure. The red isosurfaces represent the decomposed charge density of the flat (localized) band lying in the energy range from −1 60 to −1.50 eV.

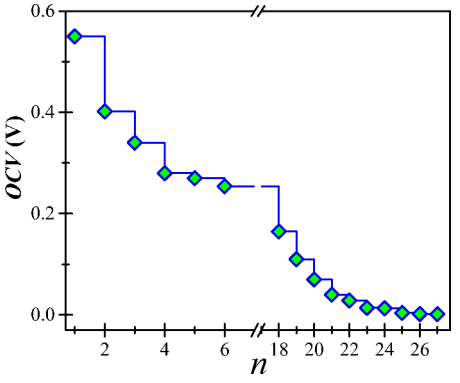

Figure 9. Electrochemical open-circuit voltage profile for the lithiated WS_2/graphene heterostructure with respect to the number of lithium added to the system.

mobility within the electrodes. Therefore, understanding the lithium diffusion barrier of the electrode material is crucial. To investigate this, we employed Climbing Image Nudged Elastic Band (CI-NEB) calculations to simulate the diffusion of Li from one adsorption site to adjacent sites. The results are presented in Figure 10 and Figure S13 (Supporting Information). Figure 10 reveals that the energy barrier for Li migration within the interlayer region is around 0.27 eV. This

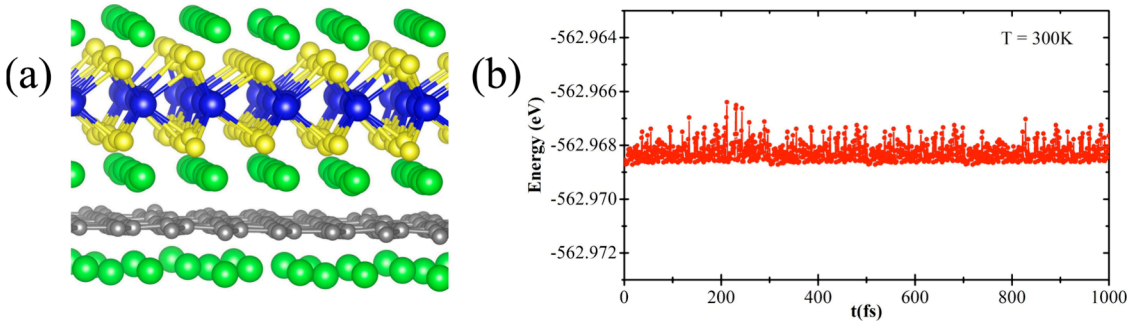

Figure 8. Ball and stick model of lithiated WS-graphene at 300 K (a, b) corresponding time step vs energy variation.

https://doi.org/10.1021/acsomega.3c06559
ACS Omega 2024, 9, 6482−6491

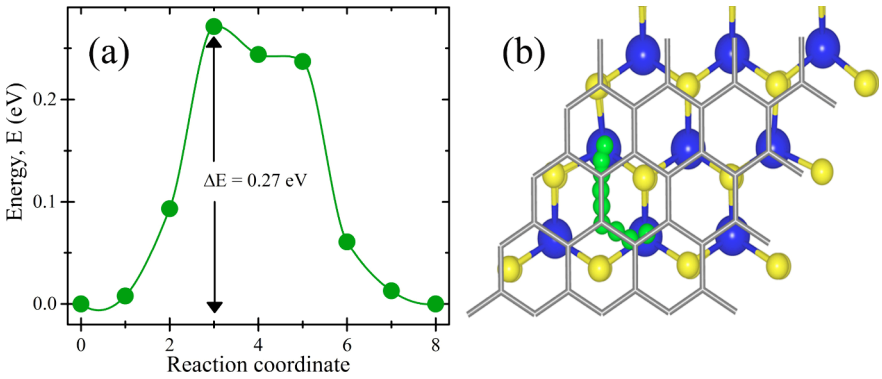

Figure 10. Energy barrier (a) and the corresponding path (b), for the diffusion of Li through the interface of WS_2/graphene heterostructure. In panel b, the movement of Li through the interface is shown by green colored balls.

relatively low barrier suggests promising Li-ion mobility within the WS2/graphene heterostructure, potentially leading to favorable charge−discharge rates.

Similarly, for other adjacent W-sites at the WS2/graphene interface, the energy barriers for Li migration fall within the range of 0.24−0.28 eV. However, at higher Li concentrations, there is a higher probability of Li adsorption on the surfaces of both WS2 and graphene. Considering this, we extended our calculations to estimate the Li-diffusion barriers on these additional sites, as shown in Figure S14 (Supporting Information). The results reveal that the barriers are 0.20 eV for Li above the top of WS2 and 0.36 eV for Li above the top of the graphene layer. Interestingly, our calculations point to an energy barrier of just 0.27 eV for Li migration through the energetically favored site within the heterostructure. This value is even lower than those of many previously reported LIB anode materials. These favorable electrochemical properties, including low lithium diffusion barriers, strongly suggest that the WS2/graphene heterostructure holds significant promise as a candidate material for next-generation LIBs.

CONCLUSIONS

In brief, using first-principles-based DFT calculations, we systematically explored the prospects of the WS2/graphene heterostructure as an anode material for LIB. The structural and electronic properties reveal that WS2 and graphene form a stable vdW heterostructure, and this material is long-lasting toward lithiation, confirmed by calculating the Li-adsorption energy. The level of lattice expansion during lithiation is low. This indicates the structural stability of the material. The structural stability of the heterostructure is highly desirable for the employment of them as electrode materials. The electronic structure of the system demonstrates that the low electronic conductivity of a single-layer WS2 has been improved by stacking with a graphene layer. In addition, the method to enhance Li adsorption in this heterostructure is also explored by B and N doping. Our results demonstrated that the B-doping in the graphene layer of the heterostructure significantly improves the Li-adsorption energy. The Bader charge and charge density analyses prove that the intercalated Li ions share their charge with both layers of the WS2/graphene heterostructure. However, the charge transfer to the WS2 was higher than that to the graphene. The electronic conductivity of the heterostructure is enhanced significantly during lithiation. The electrochemical voltage profile demonstrates that this material outperforms many reported anode materials, as proven by OCV and Li-diffusion calculations.

ASSOCIATED CONTENT

Supporting Information

The Supporting Information is available free of charge at https://pubs.acs.org/doi/10.1021/acsomega.3c06559.

(1) Ball and stick models of single-layer graphene and WS_2, (2) lattice constant optimization of the WS_2/graphene heterostructure, (3) inter layer distance vs binding energy diagram for the WS_2/graphene heterostructure, (4) band structure of single-layer WS_2 and graphene sheet, (5) charge density difference of the WS_2/graphene heterostructure, (6) adsorption of Li on various sites of the WS_2/graphene heterostructure, (7) various mode of adsorption of the Li on WS_2/graphene heterostructure, (8) various adsorption sites in the interface of the WS_2/graphene heterostructure and the corresponding Li-adsorption energy plot, (9) structural characteristics various lithiated systems, (10) adsorption of Li on WS_2 and graphene, (11) optimized structures of the highly lithiated WS_2/graphene heterostructure, (12) local structure showing the formation of W−W bonds, (13) band structures showing the splitting of the Dirac cone in the WS_2/graphene heterostructure, (14) energy barrier for the diffusion of Li through the interface of the WS_2/graphene heterostructure, and (15) energy barrier for the diffusion of Li through the surface of the WS_2/graphene heterostructure (PDF)

AUTHOR INFORMATION

Corresponding Author

T. K. Bijoy − *Indo-Korea Science and Technology Center (IKST), Bengaluru 560065, India;* orcid.org/0000-0001-7938-6601; Email: bijoyscs@gmail.com

Authors

Sooryadas Sudhakaran − *Mechanical Engineering Department, National Institute of Technology Calicut, Calicut, Kerala 673601, India;* orcid.org/0009-0009-6354-9694

Seung-Cheol Lee − *Indo-Korea Science and Technology Center (IKST), Bengaluru 560065, India; Electronic Materials Research Center, KIST, Seoul 136-791, South Korea;* orcid.org/0000-0002-9741-6955

Complete contact information is available at:

https://doi.org/10.1021/acsomega.3c06559
ACS Omega 2024, 9, 6482−6491

https://pubs.acs.org/10.1021/acsomega.3c06559

Author Contributions

The manuscript was written through contributions of all authors. All authors have given approval to the final version of the manuscript.

Notes

The authors declare no competing financial interest.

■ ACKNOWLEDGMENTS

T.K.B. is grateful to IKST for the support. S.S. is thankful for the support from NIT Calicut. All the authors extend deep gratitude to IKST for providing high-performance computing (HPC) facilities.

■ ABBREVIATIONS

LIB-lithium-ion battery; DFT-density functional theory; OCV-open-circuit voltage; GGA-generalized gradient approximation; AIMD-*ab initio* molecular dynamics; CI-NEB-climbing image nudged elastic band

■ REFERENCES

(1) Goodenough, J. B.; Park, K.-S. The Li-Ion Rechargeable Battery: A Perspective. *J. Am. Chem. Soc.* **2013**, *135*, 1167−1176.
(2) Sun, Y.; Liu, N.; Cui, Y. Promises and Challenges of Nanomaterials for Lithium-Based Rechargeable Batteries. *Nat. Energy* **2016**, *1*, 16071.
(3) Eftekhari, A. Lithium Batteries for Electric Vehicles: From Economy to Research Strategy. *ACS Sustainable Chem. Eng.* **2019**, *7*, 5602−5613.
(4) Duffiet, M.; Blangero, M.; Cabelguen, P. − E.; Delmas, C.; Carlier, D. Influence of the Initial Li/Co Ratio in $LiCoO_2$ on the High-Voltage Phase-Transitions Mechanisms. *J. Phys. Chem. Lett.* **2018**, *9*, 5334−5338.
(5) Fan, X.; Liu, Y.; Ou, X.; Zhang, J.; Zhang, B.; Wang, D.; Hu, G. Unravelling the influence of quasi single-crystalline architecture on high-voltage and thermal stability of $LiNi_{0.5}Co_{0.2}Mn_{0.3}O_2$ cathode for lithium-ion batteries. *Chem. Eng. J.* **2020**, *393*, No. 124709.
(6) Tron, A.; Park, Y. D.; Mun, J. Influence of organic additive on the electrochemical performance of $LiFePO_4$ cathode in an aqueous electrolyte solution. *Solid State Sci.* **2020**, *101*, No. 106152.
(7) Goriparti, S.; Miele, E.; De Angelis, F.; Di Fabrizio, E.; Proietti Zaccaria, R.; Capiglia, C. Review on Recent Progress of Nano-structured Anode Materials for Li-Ion Batteries. *J. Power Sources* **2014**, *257*, 421−443.
(8) Fang, Y.; Lv, Y.; Che, R.; Wu, H.; Zhang, X.; Gu, D.; Zheng, G.; Zhao, D. Two-dimensional Mesoporous Carbon Nanosheets and their derived Graphene Nanosheets: Synthesis and Efficient Lithium Ion Storage. *J. Am. Chem. Soc.* **2013**, *135*, 1524−1530.
(9) Yao, F.; Pham, D. T.; Lee, Y. H. Carbon-Based Materials for Lithium-Ion Batteries, Electrochemical Capacitors, and Their Hybrid Devices. *ChemSusChem* **2015**, *8*, 2284−2311.
(10) Ming, J.; Cao, Z.; Wahyudi, W.; Li, M.; Kumar, P.; Wu, Y.; Hwang, J. Y.; Hedhili, M. N.; Cavallo, L.; Sun, Y. K.; Li, L. J. New Insights on Graphite Anode Stability in Rechargeable Batteries: Li Ion Coordination Structures Prevail over Solid Electrolyte Interphases. *ACS Energy Lett.* **2018**, *3*, 335−340.
(11) de las Casas, C.; Li, W. A Review of Application of Carbon Nanotubes for Lithium Ion Battery Anode Material. *J. Power Sources* **2012**, *208*, 74−85.
(12) Jiang, S.; Hu, B.; Sahore, R.; Zhang, L.; Liu, H.; Zhang, L.; Lu, W.; Zhao, B.; Zhang, Z. Surface-Functionalized Silicon Nanoparticles as Anode Material for Lithium-Ion Battery. *ACS Appl. Mater. Interfaces* **2018**, *10*, 44924−44931.
(13) Novoselov, K. S.; Geim, A. K.; Morozov, S. V.; Jiang, D.; Katsnelson, M. I.; Grigorieva, I. V.; Dubonos, S. V.; Firsov, A. A. Two-Dimensional Gas of Massless Dirac Fermions in Graphene. *Nature* **2005**, *438*, 197−200.
(14) Xiong, D. B.; Li, X. F.; Bai, Z. M.; Shan, H.; Fan, L. L.; Wu, C. X.; Li, D. J.; Lu, S. G. Superior Cathode Performance of Nitrogendoped Graphene Frameworks for Lithium Ion Batteries. *ACS Appl. Mater. Interfaces* **2017**, *9*, 10643−10651.
(15) Hassoun, J.; Bonaccorso, F.; Agostini, M.; Angelucci, M.; Betti, M. G.; Cingolani, R.; Gemmi, M.; Mariani, C.; Panero, S.; Pellegrini, V.; Scrosati, B. An Advanced Lithium-Ion Battery Based on a Graphene Anode and a Lithium Iron Phosphate Cathode. *Nano Lett.* **2014**, *14*, 4901−4906.
(16) Cai, Y.; Zhang, G.; Zhang, Y.-W. Electronic properties of phosphorene/graphene and phosphorene/hexagonal boron nitride heterostructures. *J. Phys. Chem. C* **2015**, *119*, 13929−13936.
(17) Jose, D.; Datta, A. Structures and Chemical Properties of Silicene: Unlike Graphene. *Acc. Chem. Res.* **2014**, *47*, 593−602.
(18) Galashev, A. E.; Zaikov, Y. P.; Vladykin, R. G. Effect of electric field on lithium ion in silicene channel. Computer experiment. Russ. *J. Electrochem.* **2016**, *52*, 966−974.
(19) Shi, L.; Zhao, T. S. Recent Advances in Inorganic 2D Materials and Their Applications in Lithium and Sodium Batteries. *J. Mater. Chem. A* **2017**, *5*, 3735−3758.
(20) Karthikeyan, J.; Ranawat, Y. S.; Murugan, P.; Kumar, V. Borophene layers on an Al(111) surface − the finding of a borophene layer with hexagonal double chains and b9 nonagons using ab initio calculations. *Nanoscale* **2018**, *10*, 17198−17205.
(21) Bijoy, T. K.; Murugan, P. Lithiation of the Two-Dimensional Silicon Carbide−Graphene van der Waals Heterostructure: A First Principles Study. *J. Phys. Chem. C* **2019**, *123*, 10738−10745.
(22) Stephenson, T.; Li, Z.; Olsen, B.; Mitlin, D. Lithium Ion Battery Applications of Molybdenum disulfide (MoS_2) Nanocomposites. *Energy Environ. Sci.* **2014**, *7*, 209−231.
(23) Tang, Q.; Zhou, Z.; Shen, P. Are MXenes Promising Anode Materials for Li Ion Batteries? Computational Studies on Electronic Properties and Li Storage Capability of Ti_3C_2 and $Ti_3C_2X_2$ (X = F, OH) Monolayer. *J. Am. Chem. Soc.* **2012**, *134*, 16909−16916.
(24) Tan, C.; Cao, X.; Wu, X. J.; He, Q.; Yang, J.; Zhang, X.; Chen, J.; Zhao, W.; Han, S.; Nam, G. H.; et al. Recent Advances in Ultrathin Two-Dimensional Nanomaterials. *Chem. Rev.* **2017**, *117*, 6225−6331.
(25) Thangasamy, P.; Sathish, M. Rapid, One-Pot Synthesis of Luminescent MoS_2 Nanoscrolls Using Supercritical Fluid Processing. *J. Mater. Chem. C* **2016**, *4*, 1165−1169.
(26) Han, G. H.; Duong, D. L.; Keum, D. H.; Yun, S. J.; Lee, Y. H. Waals Metallic Transition Metal Dichalcogenides. *Chem. Rev.* **2018**, *118*, 6297−6336.
(27) Zhang, X.; Lai, Z.; Ma, Q.; Zhang, H. Novel Structured Transition Metal Dichalcogenide Nanosheets. *Chem. Soc. Rev.* **2018**, *47*, 3301−3338.
(28) Zhang, J. L.; Du, C. F.; Dai, Z. F.; Chen, W.; Zheng, Y.; Li, B.; Zong, Y.; Wang, X.; Zhu, J. W.; Yan, Q. Y. NbS2 nanosheets with M/Se (M = Fe, Co, Ni) codopants for Li+ and Na+ storage. *ACS Nano* **2017**, *11*, 10599−10607.
(29) Santhosha, A. L.; Nayak, P. K.; Pollok, K.; Langenhorst, F.; Adelhelm, P. Exfoliated MoS_2 as Electrode for All-Solid-State Rechargeable Lithium-Ion Batteries. *J. Phys. Chem. C* **2019**, *123*, 12126−12134.
(30) Ovchinnikov, D.; Allain, A.; Huang, Y.-S.; Dumcenco, D.; Kis, A. Electrical Transport Properties of Single-Layer WS_2. *ACS Nano* **2014**, *8*, 8174−8181.
(31) Delabie, A.; Caymax, M.; Groven, B.; Heyne, M.; Haesevoets, K.; Meersschaut, J.; Nuytten, T.; Bender, H.; Conard, T.; Verdonck, P.; et al. Low Temperature Deposition of 2D WS_2 Layers from WF_6 and H_2S Precursors: Impact of Reducing Agents. *Chem. Commun.* **2015**, *51*, 15692−15695.
(32) Toh, R. J.; Sofer, Z.; Luxa, J.; Sedmidubsky, D.; Pumera, M. 3R Phase of MoS_2 and WS_2 Outperforms the Corresponding 2H Phase for Hydrogen Evolution. *Chem. Commun.* **2017**, *53*, 3054−3057.

https://doi.org/10.1021/acsomega.3c06559
ACS Omega 2024, 9, 6482−6491

(33) Chowdhury, C.; Karmakar, S.; Datta, A. Capping Black Phosphorene by h-BN Enhances Performances in Anodes for Li and Na Ion Batteries. *ACS Energy Lett.* **2016**, *1*, 253−259.
(34) Wang, B.; Zhang, Y.; Zhang, J.; Xia, R.; Chu, Y.; Zhou, J.; Yang, X.; Huang, J. Facile synthesis of a MoS_2 and functionalized graphene heterostructure for enhanced lithium-storage performance. *ACS Appl. Mater. Interfaces* **2017**, *9*, 12907−12913.
(35) Larson, D. T.; Fampiou, I.; Kim, G.; Kaxiras, E. Lithium intercalation in graphene-MoS_2 heterostructures. *J. Phys. Chem. C* **2018**, *122*, 24535.
(36) Miwa, R. H.; Scopel, W. L. Lithium incorporation at the MoS_2/graphene interface: an ab initio investigation. *J. Phys.: Condens. Matter* **2013**, *25*, No. 445301.
(37) Eftekhari, A. Tungsten Dichalcogenides (WS2, WSe2, and WTe2) Materials Chemistry and Applications. *J. Mater. Chem. A* **2017**, *5*, 18299.
(38) Biroju, R. K.; Das, D.; Sharma, R.; Pal, S.; Mawlong, L. P. L.; Bhorkar, K.; Giri, P. K.; Singh, A. K.; Narayanan, T. N. Hydrogen Evolution Reaction Activity of Graphene-MoS2 van Der Waals Heterostructures. *ACS Energy Lett.* **2017**, *2*, 1355−1361.
(39) Wu, Y. L.; Hong, J. B.; Zhong, W. X.; et al. Auxiliary ball milling to prepare WS2/graphene nanosheets composite for lithium-ion battery anode materials. *Tungsten* **2023**, 1.
(40) Du, Y.; Zhu, X.; Si, L.; Li, Y.; Zhou, X.; Bao, J. Improving the Anode Performance of WS2 through a Self-Assembled Double Carbon Coating. *J. Phys. Chem. C* **2015**, *119*, 15874−15881.
(41) Kresse, G.; Furthmüller, J. Efficient iterative schemes for ab initio total-energy calculations using a plane-wave basis set. *Physical Review B: Condensed Matter and Materials Physics* **1996**, *54*, 11169−11186.
(42) Blöchl, P. E. Projector augmented-wave method. *Physical Review B: Condensed Matter and Materials Physics* **1994**, *50*, 17953−17979.
(43) Grimme, S.; Antony, J.; Ehrlich, S.; Krieg, H. A Consistent and Accurate Ab Initio Parametrization of Density Functional Dispersion Correction (DFT-D) for the 94 Elements H-Pu. *J. Chem. Phys.* **2010**, *132*, No. 154104.
(44) Henkelman, G.; Arnaldsson, A.; Jonsson, H. A fast and robust algorithm for Bader decomposition of charge density. *Comput. Mater. Sci.* **2006**, *36*, 354−360.
(45) Bader, R. F. W.; MacDougall, P. J.; Lau, C. D. H. Bonded and Nonbonded Charge Concentrations and Their Relation to Molecular Geometry and Reactivity. *J. Am. Chem. Soc.* **1984**, *106*, 1594−1605.
(46) Henkelman, G.; Uberuaga, B. P.; Jónsson, H. Climbing image nudged elastic band method for finding saddle points and minimum energy paths. *J. Chem. Phys.* **2000**, *113*, 9901−9904.
(47) Togo, A.; Tanaka, I. First Principles Phonon Calculations in Materials Science. *Scr. Mater.* **2015**, *108*, 1−5.
(48) Schutte, W.; De Boer, J.; Jellinek, F. Crystal Structures of Tungsten Disulfide and Diselenide. *J. Solid State Chem.* **1987**, *70*, 207−209.
(49) Amin, B.; Kaloni, T. P.; Schwingenschlö gl, U. Strain Engineering of WS_2, WSe_2, and WTe_2. *RSC Adv.* **2014**, *4*, 34561.
(50) Kang, J.; Tongay, S.; Zhou, J.; Li, J.; Wu, J. Band Offsets and Heterostructures of Two Dimensional Semiconductors. *Appl. Phys. Lett.* **2013**, *102*, No. 012111.
(51) Aliofkhazraei, M.; Ali, N.; Milne, W.; Ozkan, C.; Mitura, S.; Gervasoni, J. L. *Graphene Science Handbook:* Size-Dependent Properties. 2016.
(52) Sheng, W.; Xu, Y.; Liu, M.; Nie, G.; Wang, J.; Gong, S. The InSe/SiH type-II van der Waals heterostructure as promising water splitting photocatalyst: a first-principles study. *Phys. Chem. Chem. Phys.* **2020**, *22*, 21436−21444.
(53) Momma, K.; Izumi, F. VESTA 3 for three-dimensional visualization of crystal, volumetric and morphology data. *J. Appl. Crystallogr.* **2011**, *44*, 1272−1276.
(54) Liu, Y.; Merinov, B. V.; Goddard, W. A. Origin of low sodium capacity in graphite and generally weak substrate binding of Na and Mg among alkali and alkaline earth metals. *P. Natl. Acad. Sci. USA* **2016**, *113*, 3735−3739.
(55) Ghosh, A.; Mandal, S.; Sarkar, P. 2D Homogeneous Holey Carbon Nitride: An Efficient Anode Material for Li-ion Batteries With Ultrahigh Capacity. *ChemPhysChem* **2022**, *23*, No. e202200182.
(56) Ghosh, A.; Pal, S.; Sarkar, P. Rational Design of Two-Dimensional Porous Boron Phosphide as Efficient Cathode Material for Li and Na Ion Batteries: A First-Principles Study. *J. Phys. Chem. C* **2022**, *126*, 5092−5100.
(57) Zhang, M.; Tang, C.; Cheng, W.; Fu, L. The first-principles study on the performance of the graphene/ws2 heterostructure as an anode material of li-ion battery. *J. Alloy. Compd.* **2021**, *855*, 15743.
(58) King'ori, G. W.; Ouma, C. N. M.; Mishra, A. K.; Amolo, G. O.; Makau, N. W. Two-dimensional graphene-HfS2 van der Waals heterostructure as electrode material for alkali-ion batteries. *RSC Adv.* **2020**, *10*, 30127−30138.
(59) Peng, Q.; Wang, Z.; Sa, B.; Wu, B.; Sun, Z. Blue Phosphorene/MS2 (M = Nb, Ta) Heterostructures as Promising Flexible Anodes for Lithium-ion Batteries. *ACS Appl. Mater. Interfaces* **2016**, *8*, 13449−13457.
(60) Zhang, J.; Zhang, Y.-F.; Huang, S.-P.; Lin, W.; Chen, W.-K. BC2/Graphene heterostructure as a Promising Anode Material for Rechargeable Li-Ion Batteries by Density Functional Calculations. *J. Phys. Chem. C* **2019**, *123*, 30809−30818.

https://doi.org/10.1021/acsomega.3c06559
ACS Omega 2024, 9, 6482−6491